A GEOMETRY BASED APPROACH TOWARDS IMPROVING THE STRUCTURAL INTEGRITY OF SINGLE-WALLED TI6AL4V ALLOY FEATURES FABRICATED USING LASER DIRECTED ENERGY DEPOSITION ADDITIVE MANUFACTURING.

By

Darshan Thakkar

A THESIS

Submitted to
Michigan State University
in partial fulfillment of the requirements
for the degree of

Mechanical Engineering — Master of Science

2020

ABSTRACT

A GEOMETRY BASED APPROACH TOWARDS IMPROVING THE STRUCTURAL INTEGRITY OF SINGLE-WALLED TI6AL4V ALLOY FEATURES FABRICATED USING LASER DIRECTED ENERGY DEPOSITION ADDITIVE MANUFACTURING.

By

Darshan Thakkar

Presence of sharp turns in the deposition tool-path for Additive Manufacturing (AM) introduces heterogeneity in built-part thereby affecting structural integrity. Slower deposition speeds around turn points or corner leads to defects such as increased wall thickness, porosity, lack of fusion voids, and cracks. Such defects can be minimized by either by optimizing processing parameters or through geometry optimization. Optimizing processing parameters requires extensive and expensive set of experiments. Furthermore, it is challenging to accurately model the process and have closed loop controls because of the impracticality to include all process parameters. This work focuses on optimizing the geometry instead of the process parameters to fabricate components with minimum defects.

In this work, single walled cubical Ti6Al4V shells with sharp and rounded corners were fabricated using laser Directed Energy Deposition (DED). Cross sectional and build plane coupons were extracted from each sample for microstructure and defect analysis. Results show that inclusion of rounded corners leads to consistent deposition speeds. Defect density measurements, using optical microscope, show reduction of defects from 6.8 ± 0.35% to a virtually defect-free structure for samples with rounded corners. Results indicate that consistent deposition speed around rounded corners improved homogeneity in the resulting microstructure.

To my parents, Dhimant and Dina, for their love and support!

AKNOWLEDGEMENTS

I wish to express my heartfelt gratitude towards my advisor Dr. Himanshu Sahasrabudhe. Without his guidance, completing this thesis would not be as fulfilling as it is. I greatly appreciate the time and effort he put in making this work possible. It has been a pleasure to grow with him — from setting up the lab to manuscript submission – I am grateful for the opportunity to work with him as research assistant and for the financial support. I would also like to thank my committee members Dr. Sunil K. Chakrapani and Dr. Haseung Chung for their valuable feedback on this work. I would also like to express my gratitude to Mr. Aron O'Neil and Mr. Beytullah Aydogan for their help in setting up the lab equipment and fabricating samples.

I am very thankful to Dr. Lik Chuan Lee for his immense support and help with Finite Element Method (FEM) class. I would not have made through the degree without his support. Thank you for availability, promptness and knowledge. I also want to thank Ms. Stacy Hollon for her help in everything from admission process to the final submission of manuscript.

I also want to express gratitude for Mr. Jeff Baker and Ms. Nancy Rademacher who supported through in difficult times. I am thankful to Dr. Dhruv Bhate for his mentorship and the time he took to provide valuable insights while I was exploring career path in additive manufacturing. I'm grateful to my colleagues and friends who have supported me through this process, namely: Dr. Dinh Nguyen, Mr. Juan Sandoval, Mr. Saad Sharief, Ms. Reshma Menon, Mr. Erik Vyhmeister-Cancel, Mr. Ryan Khawarizmi, Mr. Tyler Bauder, and Mr. Kshitij Cholke.

May 2020

Darshan Thakkar

TABLE OF CONTENTS

LIST OF TABLES

LIST OF FIGURES

Chapter 1: Introduction and literature review

1.1 Background

ASTM defines Additive Manufacturing (AM) as "process of joining materials to make parts from 3D model data, usually layer upon layer, as opposed to subtractive manufacturing and formative manufacturing methodologies" [1]. AM is also referred as rapid prototyping, solid free form fabrication, digital manufacturing, and layer manufacturing among other names [2]. Using AM processes, parts are fabricated in a layer wise manner directly from the CAD model. Due to additive nature of the process, no special tools or fixtures are required regardless of part geometry. This allows fabrication of complex parts as a single structure, often not possible with conventional manufacturing [2].

While ASTM has classified AM processes into seven different categories depending energy source, feedstock material type, system setup, etc. [1], this work focuses on directed energy deposition. ASTM defines Directed Energy Deposition (DED) as "additive manufacturing process in which focused thermal energy is used to fuse materials by melting as they are being deposited" [1]. Source of thermal energy is either an electron beam or a laser, which melts the material as it gets deposited on the substrate. Feedstock material can be in powder form or wire form and is fed coaxially with the energy source. Laser directed energy deposition technique uses focused source of energy targeted to heat and melt the metal substrate, simultaneously melting and depositing the feedstock material to form a melt pool on the substrate [3]. The scanning of the energy source creates a solidified track of feedstock material deposited on the substrate. Scanning path, more commonly known as toolpath, is the path deposition head follows to fabricate the desired geometry. The process can be considered identical to welding or laser cladding but used to

fabricate 3D parts instead of joining or coating components. The process finds its use largely with metallic materials, but ceramics and metal-ceramic mixtures can also be used as feedstock materials [2-5]. Bulk net-shaped Aluminum Oxide parts have been successfully fabricated using DED demonstrating the wider possibilities with the technology [6].

AM technique and specifically laser-DED process, is a cost-competitive approach for aerospace industry where expensive materials like titanium and nickel superalloys are used in making complex components that require high buy-to-fly ratios [2]. Studies have successfully demonstrated use of DED for fabrication of bulk parts like turbine housing, mixing nozzles, and jet engines [2, 7]. Optomec has shown successful fabrication of drive shafts, gas turbine exhaust and mounting brackets produced using DED [7, 8]. AM also offers advantages like low cost and shorter lead times, which makes the process desirable for medical applications, especially in dental and orthopedic implants. Bandyopadhyay et al. has demonstrated fabrication of load bearing implants with desired mechanical properties [9]. Cellular structures and scaffolds fabricated by AM have already shown suitability for tissue regeneration [2, 10].

Laser-DED offers high deposition rates facilitating large build volumes with the ability to fabricate Functionally Graded Components (FGC) [3, 11]. Carroll et al. has demonstrated feasibility of manufacturing functionally graded Stainless-Steel components using DED [12]. Fabrication of FGC from Ti6Al4V to Invar 36 using DED AM has been demonstrated successfully, showing that it is possible to make FGC even from materials having disparate thermal properties [13]. Due to nature of deposition, a flat substrate is not required for deposition and hence the technique finds its use to repair damaged or feature additions [3]. The process is well suited for addition of features, especially single wall structures for repairing damaged such as airfoils to improve the product life cycle [2]. For example, Xue and Islam's work has demonstrated

successful addition of IN-625 alloy fins on a stainless-steel shaft [4]. Besides feature addition, Xue et al. and Kalbassa et al. have successfully demonstrated repair of components such as turbine case and tips of Inconel blades [4, 14]. Richter et al. used the process to repair Ti6242 blade to achieve superior mechanical properties compared to Ti6242 base material [15]. Nannan GUO et al. has reviewed various applications of the process in detail [2].

Present work focuses on DED for Ti6Al4V, the most commonly used Titanium alloy. Ti6Al4V (also referred as Ti64) is a two phase, alpha beta alloy offering excellent properties such as lightweight, high strength, extraordinary corrosion and fracture resistance, and biocompatibility among others [16, 17]. These properties make Ti6Al4V an attractive material for aerospace, medical, automotive and spacecraft industry [16].

1.2 Problem definition and literature review

Like any other AM technique, microstructural and mechanical properties of components fabricated by DED are dependent on processing parameters and build geometry [18, 17]. Most common defects observed are gas porosity, unmelted feedstock powder and lack of fusion voids between overlapping and side-to-side layers. Presence of defects increases the chances of part failure and reduces fatigue life [17]. The reason for formation of these defects is not well understood and there are several factors that affect defect evolution. Processing parameters such as laser power, laser spot size, powder flow rate, scan speed, shield gas, and layer thickness among others govern the thermal history and hence overall part quality. For example, higher laser power or lower scan speed results in overall higher energy input and consequently a finer microstructure from resulting high cooling rates. Powder feed rate also has a direct relation with layer thickness [17, 19]. Part quality also depends on the equipment make and the operator. Optimized parameters can help to reduce formation of common defects such as lack of fusion voids. However optimized

developed for a system of a particular make cannot be used for a system of another make. It is challenging to control for machine-to-machine induced variability through parameter optimization. Also, it is difficult to guarantee the invariance of material quality and properties.

Frazier identified that it is important to fully understand and control for variability across machines to enhance part quality and reliability [3]. Reducing process variability requires development of closed-loop adaptive control systems with sensors that can operate in a controlled environment [2]. Furthermore, rapid melting and solidification of melt pool induces a complex thermal history to the part [16]. It has been shown that layers experience at least two liquid-solid transformations [20]. This repeated melting coupled with rapid cooling rate of 10^3-10^5 K/s and large thermal gradients has profound effect on the final microstructure [3, 20]. It is challenging and would require extensive costly experiments to develop a set of time varying optimal parameters due to complex dynamics of the process. Furthermore, final properties of built part are influenced by geometry significantly, even if the optimized process parameters were time-independent [21]. It is important to understand that operator skills play a vital role in final part quality, even with the possibility of having well optimized parameters. Therefore, depending solely on optimized processing conditions for reliable and low-defect parts may not be a viable option for the laser-DED process.

One such design feature that affects the structural integrity is presence of sharp corners or turn points. When a design has sharp corner, such as a 90^o turn, it becomes necessary that the deposition speeds at corners are slower or approach zero. This happens because the motion controller has to change directions abruptly and requires deceleration in one direction followed by acceleration in another direction. With other processing parameters remaining constant, corner of the design will have a different distribution of laser energy and powder density compared to rest

of the part. Slower scan speeds lead to increased energy and powder density around the corners. There are no comprehensive studies that can recommend optimal processing parameters while also maintaining constant deposition rates [19, 21] for laser-DED AM technique. Over time, this will lead to over deposition of the material since the motion controller slows down at a corner leading to increased powder distribution per unit time. This deceleration leads to overall higher energy density at corners and hence introduces heterogeneity in the resulting microstructure. Due to additive nature of the process, such heterogeneities add up and lead to a higher defect concentration. Tang et al. has demonstrated that use of variable powder flow rate is an effective strategy to maintain comparatively uniform deposition even when disturbances like acceleration and deceleration occur [22]. However, the author also stated that it is necessary to control for other processing parameters such as laser power to obtain quality parts. Interaction of laser beam with feedstock powder to form a melt pool on the substrate is a complex phenomenon to model. Machine and operator induced variability, changing scan speeds due to presence to sharp turns in toolpath, non-uniformity in energy input, power attenuation, bulk heating, etc. are some of the major challenges that make modeling and hence control of the DED process very difficult [19, 23, 24]. Idea of having closed loop controls is also challenging because of the impracticality to include all process parameters [19]. Furthermore, these control systems are not a part of the equipment and developing one for any particular case is not a trivial task. There is a lot of work done on studying the effect of processing parameters on build quality [17-19, 21], but research is limited for defects that arise due to presence of sharp turns in deposition tool path. This work focuses on optimizing geometry instead of process parameters to obtain parts with minimum defects.

Geometry optimization can be an effective strategy for applications such as feature additions which are usually single walled structures and have turn points. Such features may be

required to be deposited on large existing components that cannot allow deposition process inside a glovebox. In such cases, it becomes challenging to have a controlled environment for use of optimized processing parameters. Because processing parameters are coupled complexly, a sub-par value for one variable can have undesirable effects on other parameters. For instance, there is high possibility of oxidation and nitridation if deposition processes carried out in an open environment. This is particularly important for titanium and zirconium-based alloys. Geometry optimization is independent of machine-to-machine variability and operator skills. Furthermore, geometry optimization does not require expensive set of experiments to develop closed loop controls and can be easily integrated in processes that are already near optimal. Current work focuses on geometry-based approach to improve structural integrity of single walled Ti6Al4V structures fabricated by laser-DED.

Chapter 2: Additive manufacturing of single walled cubical and cylindrical shells

2.1 Laser DED description

Laser Directed Energy Deposition (laser-DED) is a type of Additive Manufacturing (AM) technique. A predetermined amount of feedstock material, either powder or wire, is feed to a heat source (usually a laser) to form melt pool which gets deposited on a metallic base or substrate. The molten material is rapidly solidified and the substrate (or deposition head) moves away from the point of deposition to create a solidified track. Motion of the substrate is controlled using a motion controller defined by a predetermined toolpath. Toolpath consists of part being deconstructed into numerous layers and hatches as seen in Figure 1. Hatches can be defined as toolpaths in the XY direction or in the plane perpendicular to the build direction. This plane is also referred to as build plane. Motion controller moves the substrate in a raster-scanning fashion to deposit individual hatches. Hatches collectively become a layer. A schematic diagram shows hatch and contour scans in Figure 1. Deposition head then moves up by a distance equal to the layer thickness to repeat the process to deposit another layer of material via raster-scanned hatches. The process is repeated until the desired build geometry is achieved. A 3D geometry defined by the CAD model is thus manufactured layer by layer [2, 3].

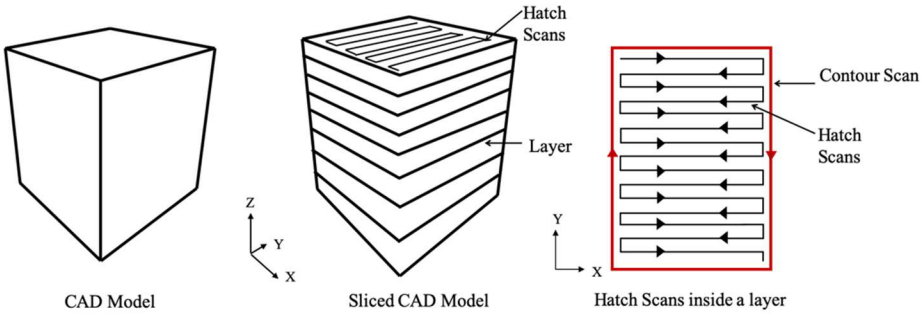

Figure 1: Slicing process for additive manufacturing using laser-DED technique.

A schematic of a typical laser-DED setup is shown in Figure 2. The deposition head is enclosed in an argon filled glovebox, a controlled environment with oxygen and moisture levels below 10ppm. Feedstock powder is loaded in an argon pressurized powder feeder as seen in Figure 2 and is fed to the deposition head by pressurized argon gas stream. Metal substrate is clamped to a motion-controlled platform facilitating motion in the XY plane. The coaxial arrangement of deposition head tips (nozzles) and laser beam facilitates maximum possible melting of feedstock powder for deposition on the metal substrate. Deposition process is carried out inside a glovebox to prevent any fire hazards, contamination and oxidation. This is particularly important for powder feedstock because powders have high surface area to volume ratio and hence are more prone to contamination.

Laser-DED equipment used in the current study has an IPG Photonics YLR-1000 fiber laser (Oxford, MA, USA), Machmotion multi-axes controller (Newburg, MO, USA), and LENS Print Engine (powder feeders and deposition head) from Optomec Inc. (Albuquerque, NM, USA).

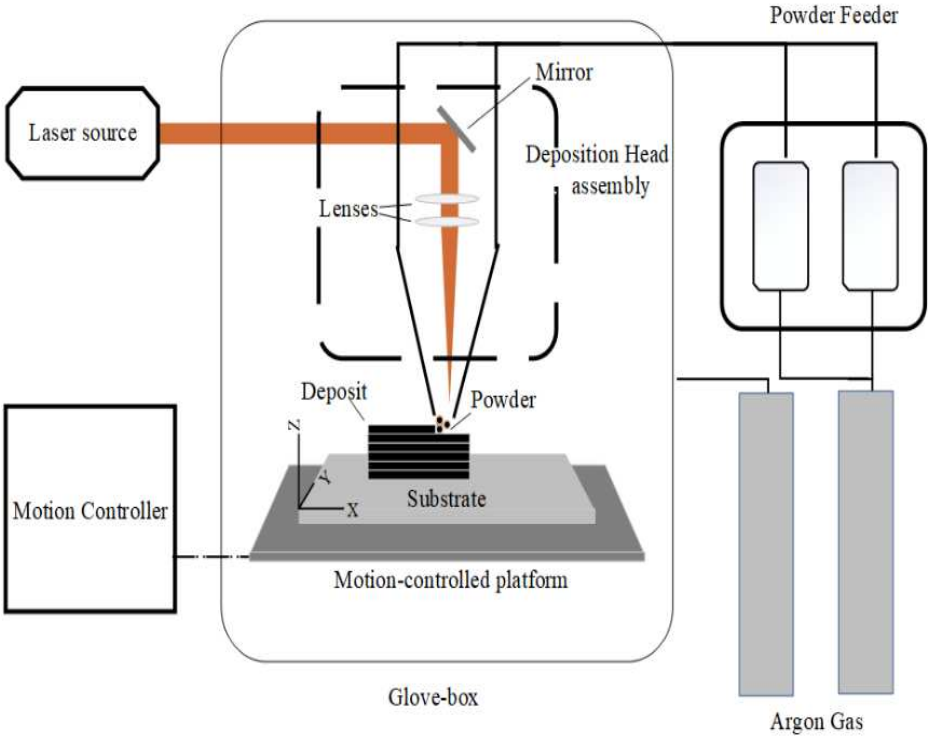

Figure 2: Schematic drawing showing typical laser-DED setup.

Laser-DED operation can be executed in two broad deposition modes: High deposition rate and low deposition rate. In high deposition rate regime, the laser power is typically greater than 500W with large laser spot size, but also circumscribed enough to prevent vaporization of the incoming feedstock powder. This is combined with larger layer thickness and larger hatch spacing and faster deposition speed. The powder feed rate is also increased. All these combined factors reduce deposition time and thus increase deposition rate. High deposition rate is appropriate for rapid deposition of large components. However, feature resolution is reduced mainly due to large laser spot size and large hatch spacing. For low deposition rate, laser power is typically below 500W with finer laser spot size. Tighter hatch spacing and slower disposition speed values thus considerably increase the deposition time. Low deposition rate is suitable for applications where a good resolution is required such as feature additions or repairs described in Section 1.1. It has been

shown that as deposition rate increases, part quality decreases [3]. This trade-off between deposition speeds and resolution is indeed an area of interest among researchers.

2.2 Processing

Commercially pure spherical Ti6Al4V powder, from Tekna Advanced Materials Inc, (Sherbrooke, QC, Canada) of particle size distribution between 45 μm and 105 μm (-100+200 Mesh) was used to deposit single walled structures using laser DED process on Ti6Al4V substrate of nominal thickness 3 mm. Processing parameters were established after several initial deposition trials with Ti6Al4V alloy as well as with other materials. To eliminate effects of changing parameters, the aforementioned processing parameters were kept constant throughout the study for all fabricated samples. Table 1 shows the processing parameters used in this study.

Initially, single walled cubical shells of side dimensions 12.7 mm (0.5 inches) and 19.05 mm (0.75 inches) were fabricated. These samples are referred as SQ-0.5 and SQ-0.75 respectively here onwards, with added description wherever possible. Table 2 summarizes the abbreviations used for designating different samples and coupons in the study. To have a control sample, a single walled cylinder of diameter 25.4 mm (1 inches). This cylindrical shell is referred as C-1. Figure 3 shows a schematic of the sample geometry for cubical and cylindrical shell.

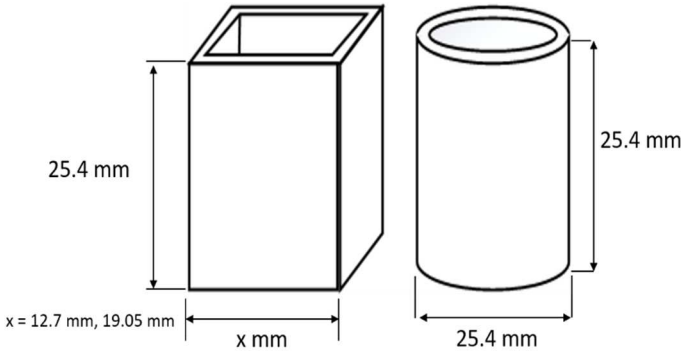

Figure 3: Schematic of single-walled shelled sample geometry to be deposited using laser-DED.

All samples have a nominal build height of 25.4 mm and were fabricated using processing parameters as summarized in Table 1. Samples were fabricated inside glove box filled with argon gas and maintained at less than 10ppm of Oxygen levels. The laser beam used has a wavelength of 1070 nm and is operated in a continuous wave configuration.

Process Parameter	
Laser power	500 W
Estimated Spot size	800 μm
Approximate Power density	822 (MW/m^2)
Travel speed	101.60 (cm/min)
Powder flow rate	6.76 (g/min)
Number of passes per layer	1.00
Layer thickness	0.3048 (mm)
Standoff/working distance	7.60 (mm)
Shield gas flow rate	20.00 (l/min)
Oxygen and moisture	<10.00 (ppm)

Table 1: Processing parameters used for the fabrication.

Length of defects (cracks, porosity, etc.) originating at corners and extending into the sample wall were calculated for cubical shells with sharp corners (SQ-0.5 and SQ-0.75) using optical microscope. An appropriate radius was chosen based on this data to fabricate cubical shells with rounded corner, also commonly referred as a fillet. Two radii, R1 and R2 of 500 μm and 1000 μm respectively, were selected for each cubical shell size. These samples will be referred as SQ-0.5-R1, SQ-0.5-R2, SQ-0.75-R1 and SQ-0.75-R2 as summarized in Table 2. Rounded cubical shells were fabricated at the same processing parameters as in Table 1.

Sample Designation	Sample Description
C-1	Single walled cylindrical shell of 25.4 mm (1 inches) diameter and 25.4 mm height
SQ-0.5	Single walled cubical shell of 12.7 mm (0.5 inches) side and 25.4 mm tall
SQ-0.75	Single walled cubical shell of 19.05 mm (0.75 inches) side and 25.4 mm tall
SQ-0.5-R1	Single walled cubical shell of 12.7 mm side and 25.4 mm tall with rounded corners of radius R1
SQ-0.5-R2	Single walled cubical shell of 12.7 mm side and 25.4 mm tall with rounded corners of radius R2
SQ-0.75-R1	Single walled cubical shell of 19.05 mm side and 25.4 mm tall with rounded corners of radius R1
SQ-0.75-R2	Single walled cubical shell of 19.05 mm side and 25.4 mm tall with rounded corners of radius R2
ZY- corner	Cross-sectional coupon extracted at the corners for cubical shells
ZY- middle	Cross-sectional coupon extracted at midway of the side for cubical shells
XY-Top	Build-plane coupon extracted near the surface of sample
XY-Middle	Build-plane coupon extracted near mid x-z plane of sample
XY-Bottom	Build-plane coupon extracted near metal substrate

Table 2: Abbreviations used for identifying different samples and coupons.

2.3 Metallography coupons preparation

Laser-DED fabricated samples were sectioned on MTI Corporations' (Richmond, CA, USA) low speed diamond saw and hot mounted in epoxy course glass filled powder. Sectioned coupons were wet ground with SiC paper from 120 grit to 1000 grit. The ground coupons were then polished using colloidal silica until they had a mirror-like finish.

Three test coupons in the build plane were extracted at different built height as seen in Figure 4. Coupons were extracted near base plate, midway at the built height and near the top surface. These sectioned coupons constituted build plane coupons or XY coupons as referred

commonly. XY-Top is used as abbreviation for XY coupons extracted at the surface and likewise, XY-Middle and XY-Bottom are used for XY coupons extracted at mid ZY plane and near substrate respectively. The abbreviations are summarized in Table 2.

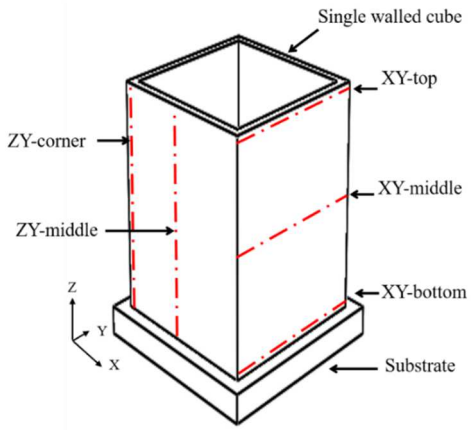

Figure 4: Schematic showing locations for coupons extraction on single walled cubical shell fabricated using laser-DED.

For each fabricated sample, cross-sectional coupons with the base plate attached, were extracted near corner and at the midway on the side edge as shown in Figure 4. The abbreviations used for identifying these cross-sectional coupons are ZY-corner and ZY-middle as summarized in Table 2. To study effects of sharp corners on defect formation more thoroughly, a complete wall section of cubical shell was extracted as discussed in section 2.4.

2.4 Defect density analysis

Defects such as porosity, cracks, and lack of fusion voids were measured using Keyence VHX- S650E (Osaka, Japan) optical microscope. All measurements were done on polished un-etched wall section at 50X magnification and within a nominal area of 4mm^2. Initially defects within 4 mm from the corner edge were considered for defect density analysis. The resulting data did not show any clear trend. However, it was observed that defects were concentrated close to corner edge and tend to reduce in distance further from corner edge. It has been reported in

literature for powder-bed fusion AM that over 87% of pores are formed within 200 µm from the turn point and are deep into the sample [39]. However, the dynamics of melt pool formation in DED are different than in powder-bed fusion process. In powder feedstock DED, a stream of argon gas carries the feedstock powder and is melted by laser to form a solidified track on metal substrate. Additionally, there is shield gas flow that cools the optics in deposition head and facilitates forced convection cooling for the melt pool. This induces turbulences in surrounding gases and increased entrapment of gases in melt pool when compared with powder-bed fusion. In current work, defects extend across the sample wall as far as 4 mm from corner edge. This could be because shield gas flow in DED adds to increased entrapped of process gas in the overheated melt pool at turn points leading to large lack of fusion voids. The wall section was hence divided into three different zones namely: 'ZX-At Corner', 'ZX-Near Corner' and 'ZX-Central' as shown in Figure 5, for defect density analysis. Boundaries separating the three zones were chosen based on results seen from initial micrographs for laser-DED processed samples.

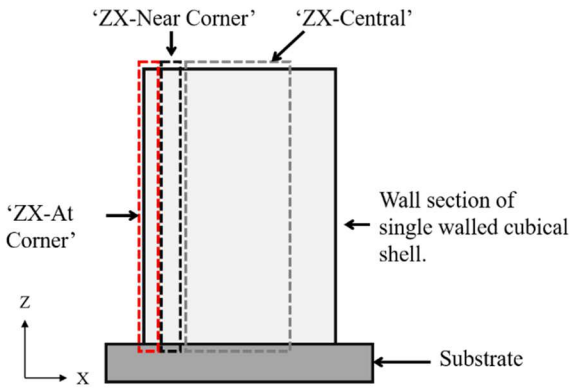

Figure 5: Defect density zones on wall section of laser-DED processed cubical shells.

Defects were manually selected to avoid false selection of scratches and small grains by the area measurement software on optical microscope. Numerous pictures at different locations were captured to allow calculation for average defect density. Measurements were done on 'ZX-

At Corner' and 'ZX-Near Corner' zones. Section 3.3 discusses the process for selection of these particular zones for defect density analysis in further detail.

2.5 Etching

Polished sections were etched for approximately 15 sec using Kroll's reagent (3ml Nitric Acid, 1ml Hydrofluoric Acid in 46ml of DI water) and were quickly washed with DI water. Etched coupons were then cleaned using an ultrasonic cleaner in ethanol solution. Optical images were captured to study microstructure evolution.

2.6 X-Ray Diffraction characterization

X-Ray Diffraction was done on as-purchased Ti6Al4V powder, polished Ti6Al4V substrate and polished DED processed coupons for phase identification. α and β phases were determined using Rigaku SmartLab (Tokyo, Japan) XRD system with Cu Kα source and Cu Kβ filter. The equipment was set at 40kV and 44mA for a 2θ scan range of 30°-80° for all measurements.

2.7 Hardness Testing

Vickers microhardness test were done on polished unetched ZY (cross-sectional) and XY (build plane) coupons using Phase2 micro-hardness tester (Upper Saddle River, NJ, USA). The microhardness tester is equipped with a standard square shaped diamond indenter and all measurements were performed at 100g load and dwell time of 15 seconds.

Chapter 3: Results and Discussions

3.1 Phase evolution after laser-DED processing of Ti6Al4V alloy

Microstructure for laser processed Ti6Al4V at room temperature is a mixture of α (hcp) and β (bcc) phases, with α phase being the dominant one. Figure 6 shows a representative optical image of microstructure for laser DED processed Ti6Al4V. The image was taken on cross-section coupon (ZY - corner) extracted on cubical shell with 0.5 inches side with sharp corner (SQ-0.5 sample). Identical microstructure was seen on cross-section coupons from other laser-DED fabricated samples in the study. Microstructure evolution in three different location on ZY- corner coupon is shown. The darker phase is the β phase. α phase has a lighter contrast compared to α' phase as seen from Figure 6. Rapid cooling rates in DED process leads a change from colony type of microstructure to martensite α' which can be identified by rectangular grid like structure. Presence of martensite α', as seen in Figure 6 and Figure 7, verifies that the deposited geometry experienced rapid cooling. Also, as seen in Figure 6(a), elongated columnar grains, referred as prior β grains, grow in the direction opposite to thermal gradient, which occurs due to conductive heat transfer downward into the cooler substrate. The columnar grains are enclosed by α grain boundaries as shown in Figure 6(c). A transition from a colony structure at the bottom to a lamellar structure at the top is observed.

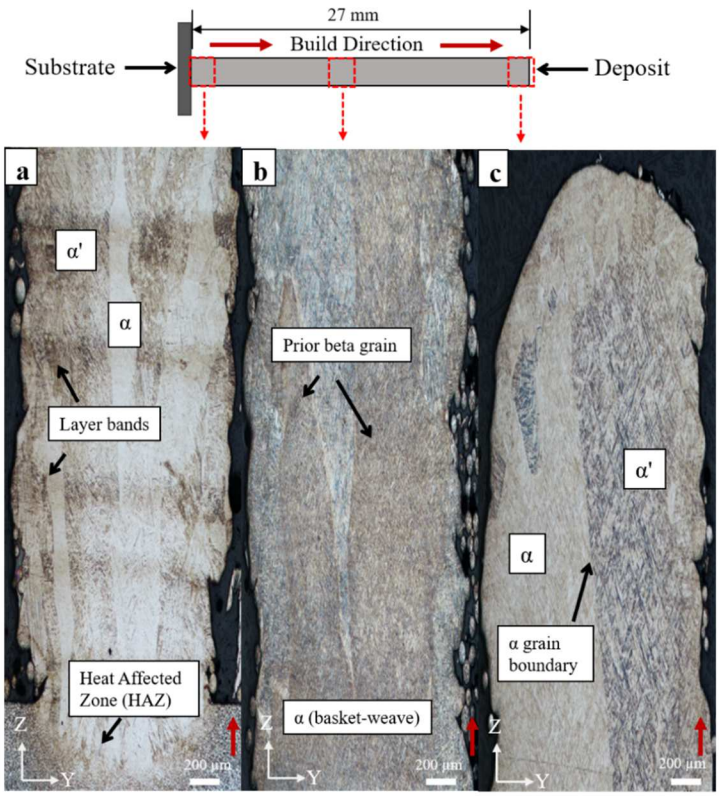

Figure 6: Microstructure of DED processed Ti6Al4V as viewed from the side (cross-sectional view) (a) bottom, (b) central, and (c) top region. Red arrow indicates build direction.

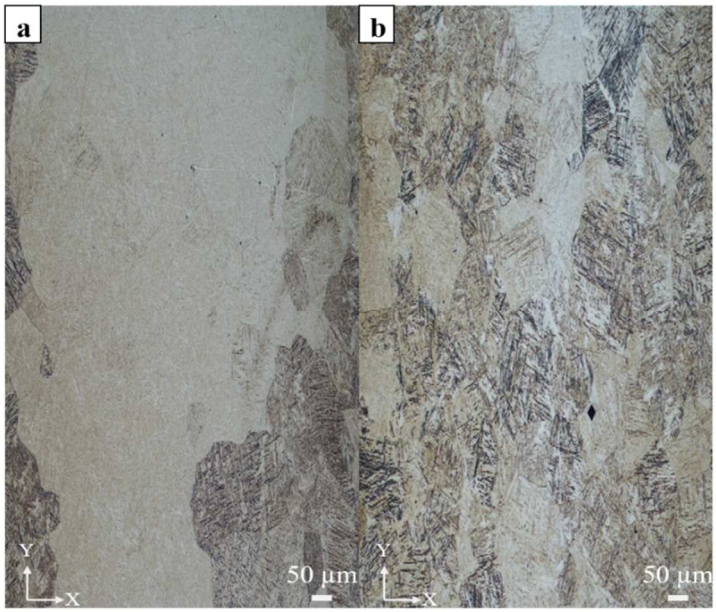

Figure 7: Microstructure of laser processed Ti6Al4V on XY plane (a) bottom and (b) top region.

As seen in Figure 7, microstructure varies with build height. Microstructure observed near the substrate, Figure 7 (a), is finer than one observation near the top surface of deposit, Figure 7 (b). Resulting microstructure at top is also relatively more martensitic than at the bottom. The microstructure varies from grain to grain and can be seen clearly in Figure 7 (a).

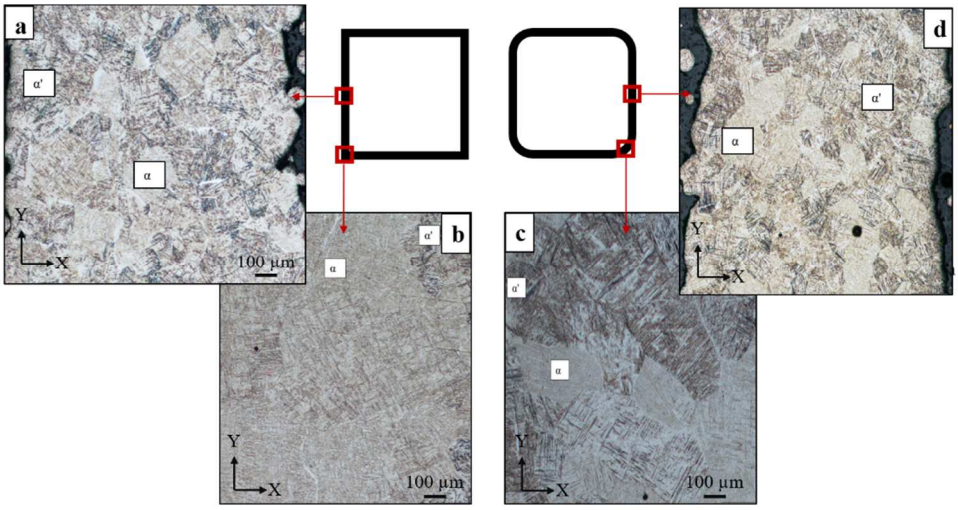

Figure 8: Microstructure of laser processed Ti6Al4V on XY plane for cubical shells (a) between sharp corners, (b) on sharp corner, (c) between rounded corners, and (d) on rounded corner.

Figure 8 shows a representative image of microstructure evolution on XY-Top coupons for cubical shell with sharp and rounded corners. The optical images are captured on XY-Top coupons for both shells to have even comparison. As seen from Figure 8, the resulting microstructure between corner locations, Figure 8(a) and Figure 8(d), is identical for shells with rounded and sharp corner. This was expected because of consistent deposition speed, and hence uniform processing parameters, between corners. However, there is difference in microstructure seen on sharp corner Figure 8(b) and rounded corner Figure 8(c). Slower deposition speeds at sharp corners, discussed in detail in section 3.7, led to increases heat input per unit time. Delayed solidification and decreased cooling rate led to decreased transformation of α+β to metastable α'.

For rounded corners, consistent deposition speeds led to uniform energy input per unit time and the resulting microstructure, as seen in Figure 8(c), is identical to microstructure seen between corners on Figure 8(a) and Figure 8(d).

High cooling rate experienced in DED processing, led to transformation of α+β phases to fine martensite structures. Hexagonal closed packed (hcp) martensite, a metastable phase, forms because rapid cooling rates do not allow the material to reach equilibrium state during solidification. It is commonly referred as α' as reported previously. Presence of α and β phases on substrate, feed-stock powder and laser-DED processed samples is confirmed from 2θ peaks obtained by X-Ray Diffraction (XRD) as shown in Figure 9 and 10. High cooling rate can also create micro strain in the built parts. Shifting of peak 2θ positions for laser processed samples is known to indicate presence of this strain. Also, broadening of diffraction peaks indicates non-uniform micro strain [25]. Absence of any major shifting or broadening, as seen by comparing Figure 9(a) and Figure 10, confirms that the strain is negligible and should be uniform over built part if present at all. Results obtained for laser-DED processed samples are representative for laser processed Ti6Al4V as reported elsewhere [25, 26].

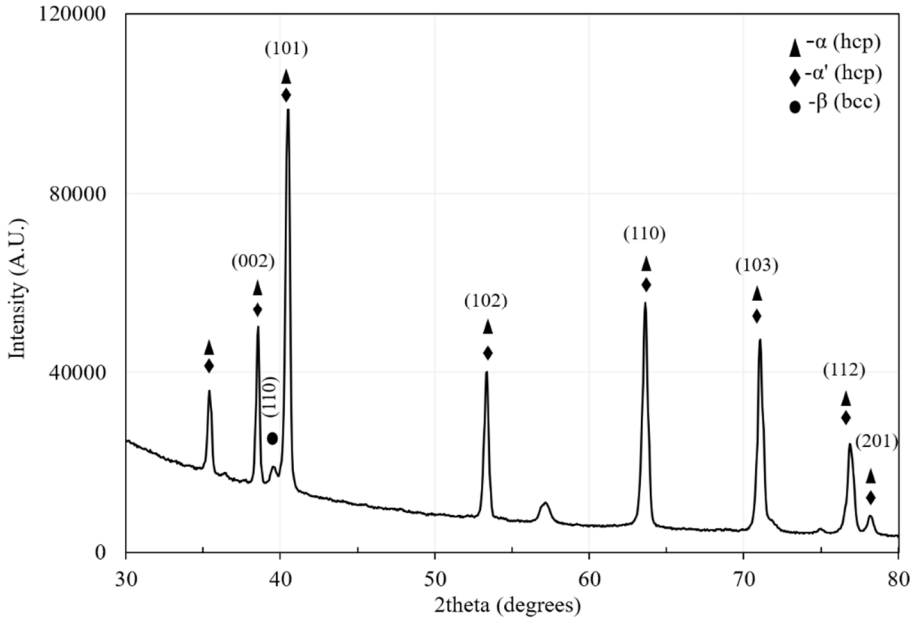

(a)

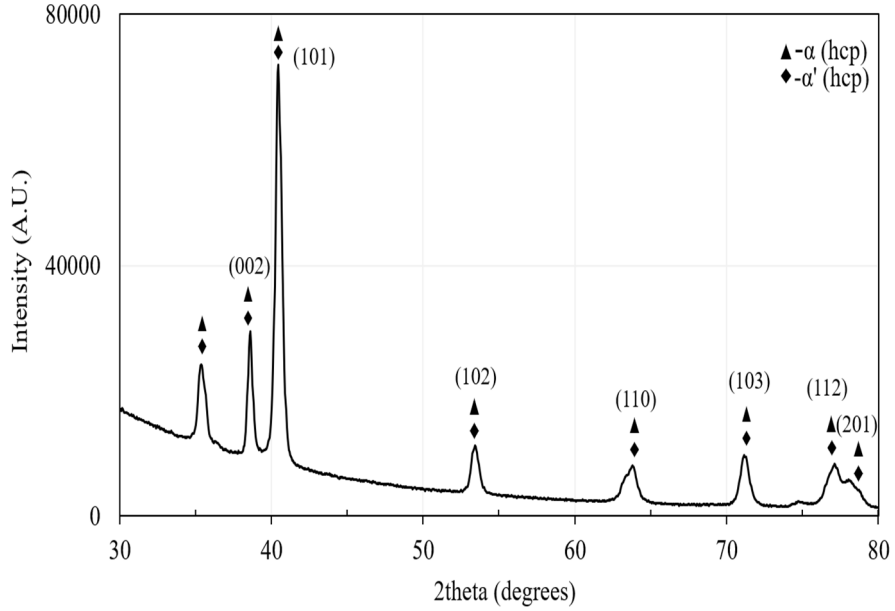

(b)

Figure 9: X-ray diffraction analysis of (a) Ti6Al4V substrate and (b) Ti6Al4V powder

Most of the peaks in Figure 10 can be assigned as α/α' phase. It is difficult to distinguish between α and α' phases because both have similar crystalline structure and lattice parameters [26] and therefore XRD peaks are commonly non-distinguishable.

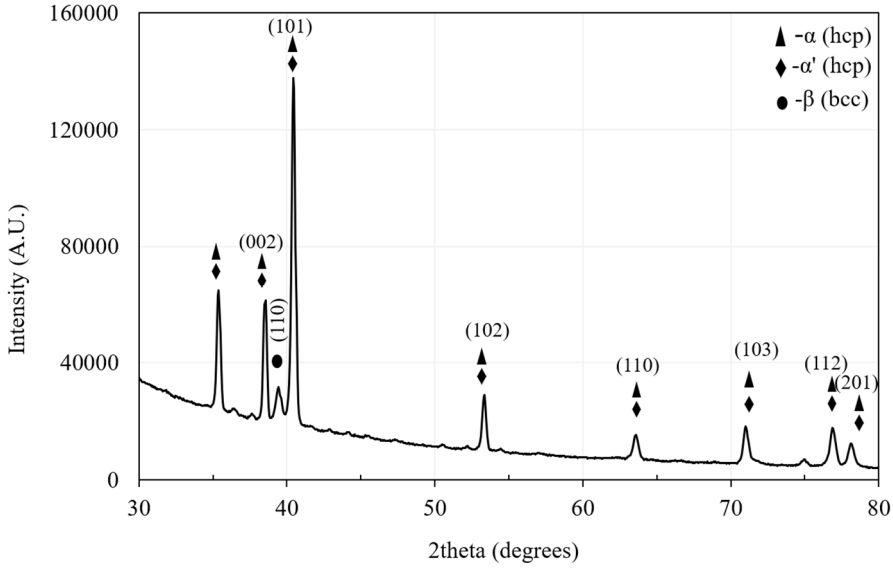

(a)

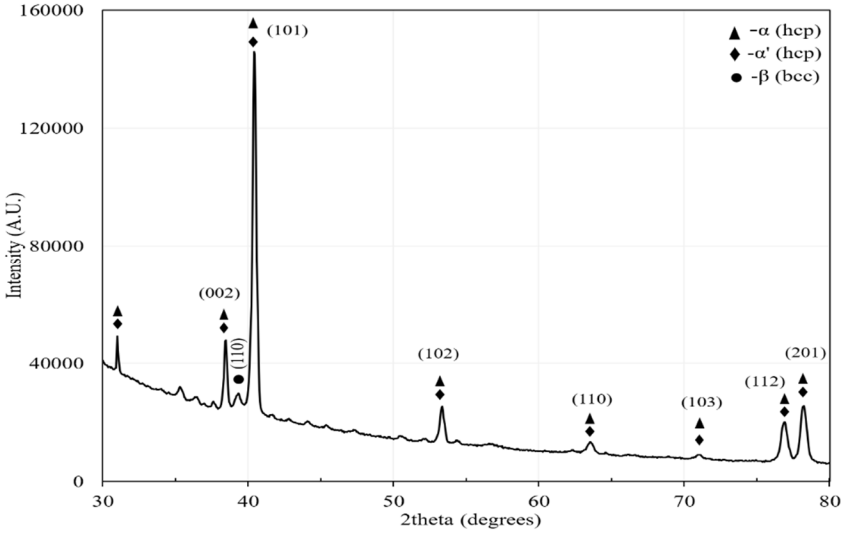

(b)

Figure 10: X-ray diffraction analysis of laser-DED (a) Cylindrical shell and (b) Cubical shell.

3.2 Microhardness analysis

3.2.1 Cubical shells with sharp corner and cylindrical shell

Vickers microhardness tests were done on cross-sectional coupons (ZY- corner and ZY-middle) and the three XY coupons (XY-Top, XY-Middle and XY-Bottom) extracted from cubical shell of base side 0.5 inches with sharp corner (SQ-0.5), cubical shell of base side 0.75 inches with sharp corner (SQ-0.75), and cylindrical shell (C-1) samples. Table 3 below shows results obtained for hardness tests. Comparatively higher value of hardness was observed in Heat Affect Zone (HAZ) on laser processed substrate. The hardness of as-received Ti6Al4V substrate was 346± 22.4 HV0.1, whereas average hardness in the HAZ is 392± 8.9 HV0.1. Generally, XY-Bottom coupons show higher hardness values compared to XY-Top and XY-Middle as seen in Table 3. Otherwise average hardness remains comparable throughout different samples regardless of location or distance from the base plate.

Sample Abbreviation	Coupon code	Average Hardness (HV0.1)
C-1	ZY- corner	325± 17.9
	XY-Top	339± 10.1
	XY-Middle	345± 9.5
	XY-Bottom	363± 9.3
SQ-0.75	ZY - corner	318± 8.9
	ZY- middle	346± 4
	XY-Top	317± 6.6
	XY-Middle	312± 6.8
	XY-Bottom	347± 9
SQ-0.5	ZY- corner	337± 23.9
	ZY- middle	335± 12.2
	XY-Top	332± 15.6
	XY-Middle	319± 12.1
	XY-Bottom	355± 8.7

Table 3: Hardness values for laser-DED fabricated cubical and cylindrical shells.

3.2.2 Cubical shells with rounded corners

Vickers microhardness tests were also done on coupons from cubical shells of same side dimensions but with rounded corners. Hardness results for cubical shells with rounded corner are summarized in Table 4. Trends similar to shells with sharp corners are observed for shells with rounded corner as seen from the data in Table 4.

Sample Abbreviation	Coupon code	Average Hardness (HV0.1)
SQ-0.5-R1	ZY-corner	343± 16
	ZY- middle	346± 16
	XY-Top	338± 14.6
	XY-Middle	332± 6.6
	XY-Bottom	364± 13.9
SQ-0.5-R2	ZY-corner	332± 19
	ZY- middle	332± 24
	XY-Top	331± 12.3
	XY-Middle	324± 10.1
	XY-Bottom	362± 5.3
SQ-0.75-R1	ZY- corner	348± 14.5
	ZY- middle	347± 17.8
	XY-Top	345± 8.8
	XY-Middle	349± 8.7
	XY-Bottom	368± 12.9
SQ-0.75-R2	ZY- corner	337± 14.8
	ZY- middle	335± 14.6
	XY-Top	n/a*
	XY-Middle	342± 14.5
	XY-Bottom	354± 8.9

Table 4: Hardness values for laser-DED fabricated rounded cubical shells.

*- sample not fabricated due to processing issues, hardness expected to follow trend.

3.3 Defect density calculations

Defect density can be defined as the ratio of area of defects in selected area to the total selected area. Current work focuses primarily on defects arising due to presence of sharp turns points in part design. Wall section was divided into three zones: 'ZX-At Corner', 'ZX-Near Corner' and 'ZX-Central' zone as discussed in section 2.4 and shown in Figure 11 below.

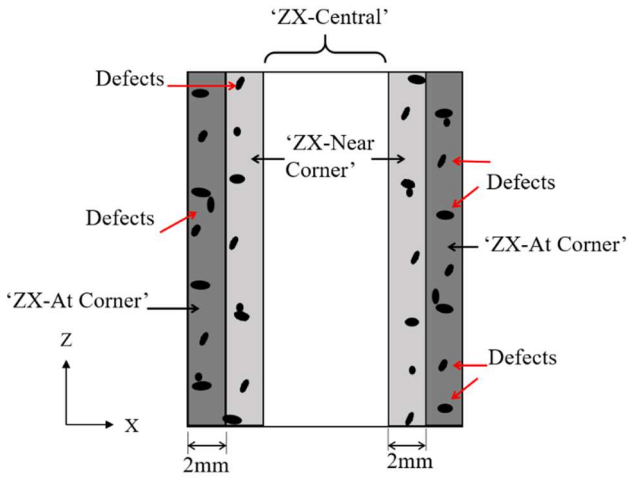

Figure 11: Defect density zones for laser-DED processed single-walled cubical specimens.

Defects such as porosity, lack of fusion voids, etc. are expected in any additively manufactured part. Such defects can also occur in 'ZX-Central' zone. However, deposition scan speeds, and hence processing conditions, remain nearly constant in the 'ZX-Central' zone because there are no turn points to cause differential speeds. Defects occurring in this zone can be reduced by optimizing processing parameters and not through geometry-based approach because 'ZX-Central' zone is simply a straight-line deposit. Therefore, defects seen in 'ZX-Central' zone are not analyzed in the current work. To estimate the range to categorize defects either as a 'ZX-At corner' defect or a 'ZX-Near corner' defect, average extent of defects from corner edge into the wall section was calculated for the shells with sharp as well as rounded corners. Based on extent of defects, it was decided that defects within 2 mm from corner edge and across the sample wall

could be a good choice to be considered as 'ZX-At corner' defects. Defects in 2 mm to 4 mm zone, measured from corner edge, should be considered as 'ZX-Near corner' defects. Defects occurring beyond the 4 mm range, and hence in 'ZX-Central' zone, were not taken into consideration for defect density analysis as discussed. Figure 11 shows the three different zones for a wall section of cubical shell. Defect density results, expressed as area percentage, are summarized in Figure 12 and 13 below.

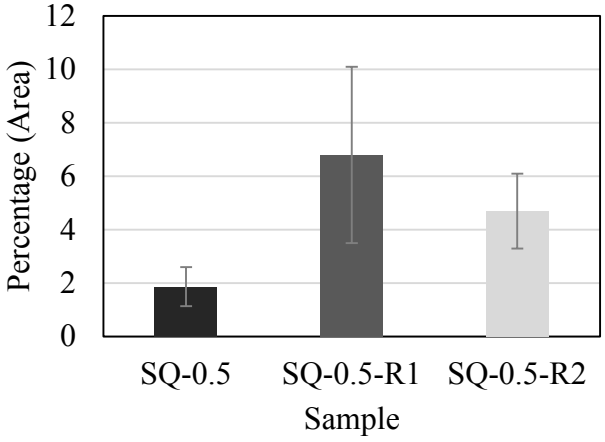

(a)

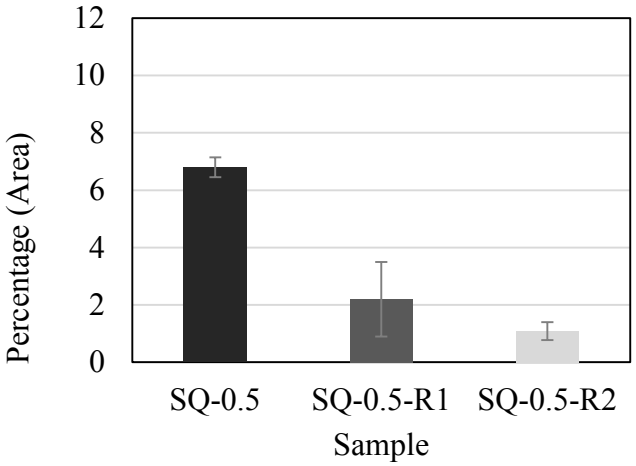

(b)

Figure 12: Defect density calculations in 0.5 inches shells (a) 'ZX-At Corners' and (b) 'ZX-Near Corners' zones.

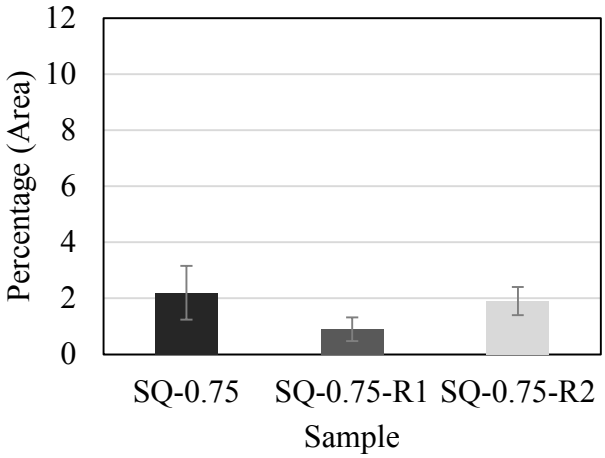

(a)

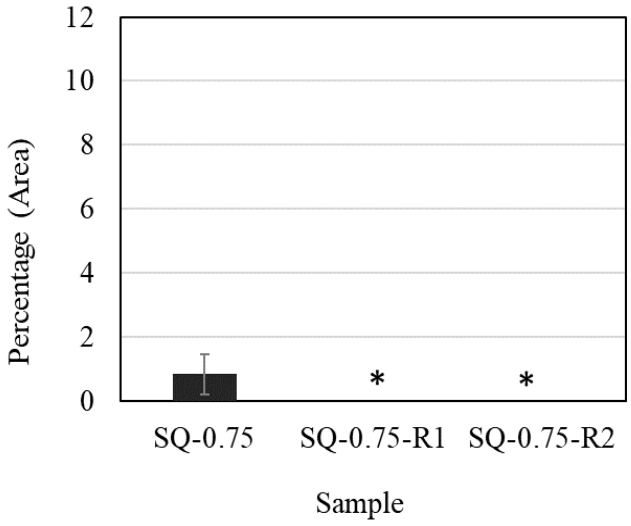

(b)

*- no defects observed, defect density measurements are nearly 0.0%

Figure 13: Defect density calculations in 0.75 inches shells (a) 'ZX-At Corners' and (b) 'ZX-Near Corners' zones.

From Figure 12 (a) and 13 (a), it clear that there no clear trend seen for defect density measurements in 'ZX-At Corner' zone (≤ 2 mm from corner). However, for measurements done in 'ZX-Near Corner' zone (2-4 mm from corner), shown in Figure 12 (b) and 13 (b), substantial reduction in defects is observed for shells for both sizes. Only one major defect was seen in the

‘ZX-Near Corner’ zone on 05-SQ, which accounted for over 6.8% of total defect density. Defect density has reduced from 6.8± 0.35 % to 1.09± 0.3 % for the cubic shells of 12.7 mm (0.5 inches) side and virtually defect free ‘ZX-Near Corner’ zone from 0.82± 0.6 % for the cubic shells of 19.05 mm (0.75 inches) side.

3.4 Single wall deposit thickness

Wall thickness measurements, using optical microscopy, were done on polished cross-sectional coupons (ZY-corner and ZY-middle) for all fabricated samples. Wall thickness was measured on at least 4 cross sectional coupons every 2-3 mm intervals to get averaged wall thickness value. Wall thickness is consistent across samples and the average values on ZY- corner and ZY- middle are 1.73 mm and 1.60 mm respectively. Slightly higher wall thickness near corner possibly explains a higher powder density per unit time due to reduced speeds.

3.5 Single wall layer thickness

Optical microscope was used to measure layer thickness on polished and etched cross-sectional coupons (ZY-corner and ZY-middle). Layer bands can be identified distinctly as seen in Figure 6(a). Measurements were done on at least 10 cross sections coupons (from sharp and rounded corner shells combined) to get averaged layer thickness value. Layer thickness is comparable across all the samples with an average value of 427±20 microns.

3.6 Powder catchment efficiency

In a powder feed DED process, not all of the powder blown through nozzles get fused into the component. Powder scattering and non-convergence in powder distribution due to turbulence in the melt pool leads to powder particles being rejected. Powder catchment efficiency can be

defined as the ratio of weight of fabricated sample to total weight of powder blown initially. For all the fabricated samples, average powder catchment efficiency of 32.34% was measured.

3.7 Discussions

Ti6Al4V is an allotropic metal whose microstructure is characterized by size and arrangement of α and β phases. β transus temperature, approximately 995 °C for Ti6Al4V, is defined as the transition temperature where α+β phases start transforming into β phase. Rapid cooling rates in DED processing leads to transformation of α+β colonies to martensite α' which are verified by a rectangular grid structure as seen in Figure 6 (c) [27]. In general, resulting microstructure is lamellar with a mix of finer and coarser grains. It is observed, from Figure 6, that the number of grains decreases with height but grain size increases. Also, microstructure varies to some extent from grain to grain as seen in Figure 7 (a). Thermal gradient, in the direction opposite to build-direction, exist in the part during deposition and occurs due to conductive heat transfer into the cooler substrate. As seen from Figure 6, grains grow epitaxially across the layers in the direction opposite to thermal gradient and can be explained by presence of thermal gradient as reported in literature [16, 27].

Sequential heating and cooling in AM results in formation of layer bands as observed in Figure 6(a). These bands do not correspond to liquidous lines but to β transus temperature lines as reported in literature [28]. These bands are derived from β transus lines of two or more subsequent re-melting of previously deposited layer [28, 29]. Absence of bands in the top region implies that the top part of the deposit experienced only partial re-melting with one cooling step. This differential cooling explains the finer microstructures seen near the substrate, Figure 7(a), and coarser microstructure near the top surface of the deposit in Figure 7(b). Bottom part also has a large grain size due to the fact it experiences heating and re-melting effects from deposition of

subsequent layers with rapid cooling through cooler substrate. Since cooling rates are expected to decrease from bottom part to the top surface during deposition process, each layer has a different thermal history associated with it. Also, Ti6Al4V has a relatively low thermal conductivity (approximately 7 $Wm^{-1}K^{-1}$ at room temperature) for a metal, so the heat transfer rate can get even slower with increasing build height [16]. Colony-like structures are known to form at slower cooling rates whereas, high cooling rates lead to martensitic hcp or α' [28]. A mix of basket weave and colonies is seen in the top region of the deposit, Figure 6(c), suggesting comparatively slower cooling rates at the top than for the remaining part. This differential cooling rates across the sample introduces heterogeneity in the resulting microstructure.

Hardening during laser deposition can occur either due to solid solution hardening, dislocation hardening, or by boundary hardening mechanisms [27]. It is expected to get a hardness gradient occurring due to different cooling rates as reported in literature [30]. Brandl et al. found that hardness decreases slightly from top to bottom of the deposit [27, 31]. Other studies in AM for Ti6Al4V alloys have however reported consistent hardness values regardless of distance on the deposit from substrate [32].

Hardness values on as-received substrate and laser processed Ti6Al4V samples are comparable with a representative average of 335± 17.5 $HV_{0.1}$. A 13% increase in hardness was observed in HAZ on laser processed substrate when compared to as-received substrate. As seen in Figure 6(a), HAZ is characterized by fine microstructure, which results in higher hardness values as reported in literature [30, 33, 34]. Unlike bulk samples where cooling rates would decrease progressively with build height, hollow samples facilitate cooling by convection more readily to maintain consistent cooling rates throughout deposition. Since the samples fabricated in this study were single walled cubes and cylinders, with shield gas facilitating forced convection, it is

expected that cooling rates remain comparable across layers during deposition without large thermal gradients. This can be seen in the resulting microstructure from Figure 6(a) where the globular microstructure transforms into a columnar microstructure right after first layer and columnar microstructure grows epitaxially throughout the built height. Results obtained for hardness measurements on cross-sectional coupons (ZY-corner and ZY-middle) hence do not show large variations in hardness value, except that the refined microstructure in HAZ results in higher hardness. A comparable value in hardness across the deposited sample indicates that thermal gradient is not large enough to introduce any gradient in hardness values.

Because DED process is similar to welding, it is reasonable to refer to existing modeling work in welding. It is obvious and has been demonstrated that weld (scan) speeds have a direct relationship with heat input [35, 36]. In terms of microstructure, lower scans speeds tend to produce larger grain size [36]. Inspired from existing modeling work, Wang et al. [37] has proposed a parameter n that encapsulates scan speed (v), thermal diffusivity (a) and the net heat input (Q-Q^C) to the part. This dimensionless operating parameter is expressed as in Eq. (1),

$$n = \frac{\eta(Q-Q^C)v}{4\pi a^2 \rho c_l (T_m - T_0)} \tag{1}$$

where η denotes the laser absorption efficiency, ρ is the melt density (kg·m^{-3}), T_m is the melting temperature (K), T_0 is the initial temperature (K), a is thermal diffusivity (m^2·s^{-1}) and c_l (J·kg^{-1}·K^{-1}) is the melt specific heat. It is important to note that powder would not melt if the supplied laser heat input Q (W) is less than the critical value Q^C (W) required for melting. Cross-sectional area A (m^2) of the melt pool can now be approximated as a linear function parametrized by dimensionless operating parameter n as in Eq. (2) when scan speed v is expressed in m·s^{-1},

$$A = \beta \frac{\eta(Q-Q^C)}{\pi \rho c_l (T_m - T_0) v} \tag{2}$$

To verify if Machmotion multi-axes controller used in the study actually accelerates and decelerates at sharp corners, a plot of velocity vs time for one complete layer was generated manually by recording real-time speed values displayed on the controller screen. Figure 14 shows speed of the controller during deposition of one complete layer for a cube of one-inch side length. Scan speed was set to 101.6 cm/min (40 inch/min). As seen from the plot, controller accelerates and decelerates at each corner of cubical shell. Data from the log file reveals that controller decelerates as it approaches the corner and comes to a complete stop at the turn point. After making the turn, deposition head starts accelerating in the direction defined by toolpath.

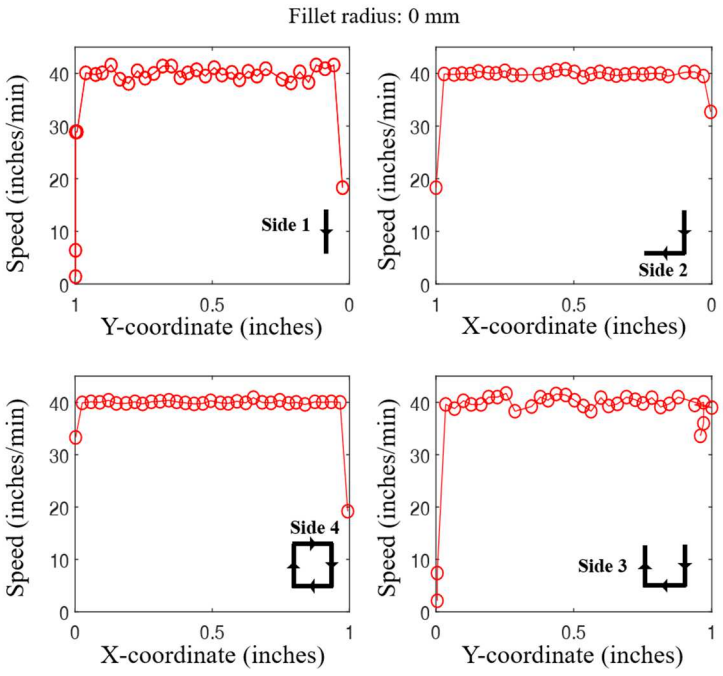

Figure 14: Velocity plots for one-inch cube with sharp corners.

It is clear from Eq. (2) and Figure 14 that slower deposition speeds at corners could lead to comparatively higher cross-section area and over deposition at the corners. This uneven clad height gets amplified as the built height of part increases. It is known that decrease in scan speed results in increased local temperatures. Benyounis et al. studied the effects of welding speeds and other

parameters on heat input [38]. The authors concluded that deposition speed (v), second order deposition speed (v) and the integration of deposition speed with laser power ($v \times Q$) have most impact on heat input. Heat input is inversely related to scan speed and is most important parameter to influence Heat Affect Zone (HAZ) width. Furthermore, higher heat input, caused by slow scan speed, produces larger grainer size causing to introduce microstructural heterogenicity in the part [19, 35].

Because controller has to change directions to deposit on the adjacent side of the shell, deposition speed must approach zero at corners. To achieve near constant speed deposition at corners without complete stopping of the motion controller, a cubical shell with rounded corner was proposed. This is essentially a cubical shell with fillets added to the corner edges. To verify if proposed design produces anticipated result of constant deposition speeds throughout, a plot of velocity vs time for one complete layer was obtained as shown in Figure 15. It is important to note that the fillet radius of 0.2 mm is a conservative choice and was chosen an as example for generating velocity plots. It is expected that higher values of fillet radius will led to improved consistency in speeds at turn points.

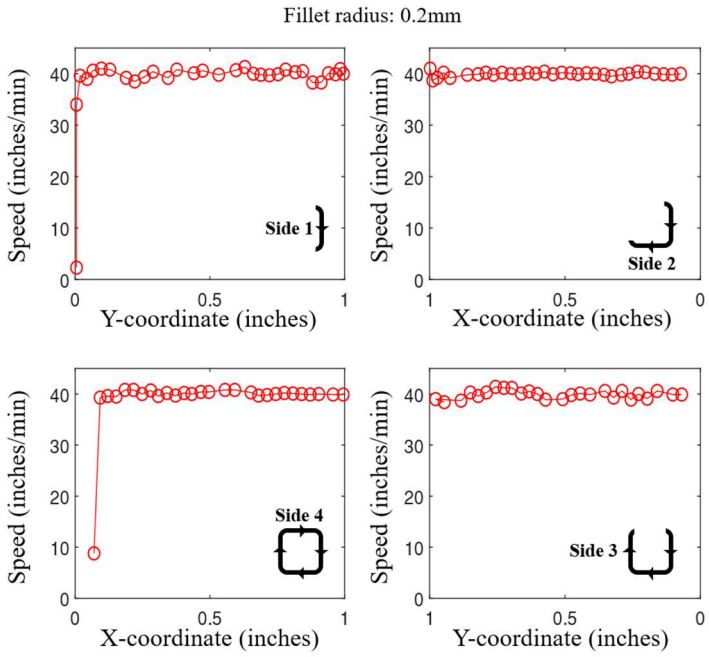

Figure 15: Velocity plots for one-inch cube with rounded corners.

As seen from Figure 15, scan speed remains nearly constant around rounded corners and drops only after a layer has been deposited completely. Inclusion of fillet at the corner edges mitigates the problem of slower deposition speeds at corners. Figure 16 shows as-built 0.5 inches cubical shell samples with and without rounded corners.

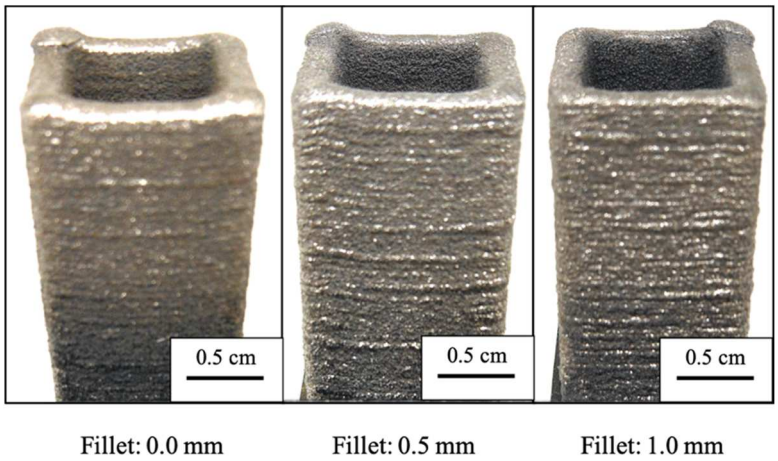

Figure 16: As-built single-wall cubical shells using laser-DED with 0.5 inches side.

Figure 16 shows that inclusion of fillet radius did not alter macroscopic appearance of samples. However, measured microscopic defects such as porosity, lack of fusion and cracks were reduced drastically on cubical shells with rounded corners as reported in Figure 12 (b) and 13 (b).

Slower deposition speeds at corners leads to increased powder density per unit time because powder flow rate is kept constant throughout the deposition process. It is important to understand that layer thickness is directly proportional to powder flow rate and laser energy intensity is inversely proportional to deposition speed [17]. From Eq. (2), it can be concluded that all variables expect the scan speed v would remain nearly constant during deposition owing to the fact heat supplied and feedstock material are same throughout in this work. Hence cross-sectional area of melt pool is dependent largely and inversely on scan speeds. Slower scan speeds at turn points led to increased cross-sectional area of melt pool, which led to increased cross-sectional area of solidified melt pool. This possibly explains by 7.5% increase in wall thickness on the ZY- corner coupons compared to ZY- middle coupons extracted from samples with sharp corners. Wall thickness on ZY- corner coupons is still more than on the ZY- middle coupons on samples with rounded corners even though deposition speeds are nearly constant. However, increase in wall thickness at ZY- corner has reduced to 5.5% for rounded corners from the initial 7.5% for samples with sharp corners. There are no literature works measuring variation of wall thickness at turn points such as sharp corners. There is a possibility that percentage values vary depending on the location for ZY- corner coupon extraction. Percentage values, although measured from at least 4 cross-sectional coupons, are hence meant to provide only a general idea of changing wall thickness.

Pores are formed when excessive energy is imparted to the melt pool and subsequent entrapment of process gas. It has been reported in literature that these pores are usually more pronounced in areas where there is decrease in scan speed or increase in laser power [39]. Increase

in energy input, either by reduced scan speeds or increased laser power, tends to overheat the melt pool. Overheated liquid metal traps the surrounding argon into the void to form pores. This is especially more critical for DED process because of presence of shield gas that is targeted at the melt pool. This leads to increased gas entrapment and pore formation. Lack of fusion voids are formed due to improper bonding between successive layers. Lower laser energy and faster scan speeds are known to introduce lack of fusion voids [40]. Rapid acceleration and deceleration at turn points causes instability in the melt pool solidification dynamics. Insufficient time for solidification and bonding leads to formation of lack of fusion voids. Cracks are formed due to high scanning speeds and residual stress arising from high thermal gradients [41,42]. Studies on pore formation have reported that pores are primarily formed at laser turn points and are more concentrated within 200 μm of turn point. It has been reported that as scan speed decreases while approaching a turn or a sharp comer, increased energy density per unit time leads to overheating of melt pool and increased depression depth on previously deposited layers [39].

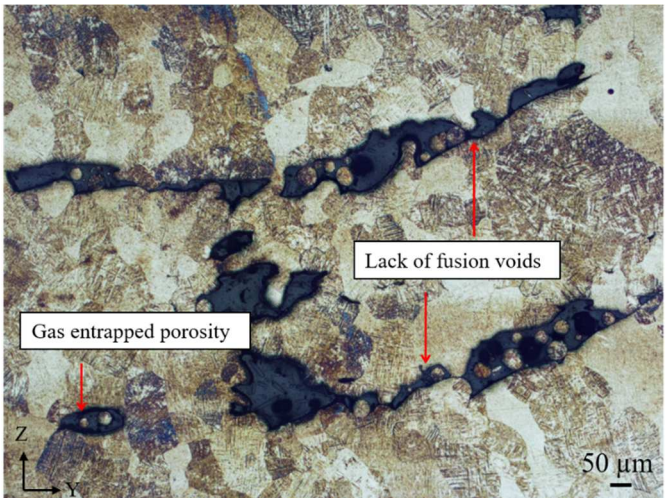

Figure 17: Porosity and lack of fusion defects in 'ZX-Near Corner' zone on cubical shell of 0.5 inches side with sharp corner (05-SQ) wall section.

Figure 17 shows lack of fusion voids and porosity seen on the wall section extracted from cubical shell with sharp corner of 0.5 inches side length (05-SQ). Figure 17, captured in 'ZX-Near Corner' zone, shows that these defects are as long as 2 mm and can greatly increase chances of part failure. After turning around sharp corners, the deposition head accelerates to programmed speed as seen in Figure 14. This rapid acceleration leads to the collapse of the depression so quickly that the overheated melt pool traps the surrounding argon to form pores [39]. Formation of large voids and pores in cubical shell with sharp corner can be verified in Figure 17.

By having rounded corners, deposition speeds are consistent thereby leading to uniform energy density. Prevention of changing scans speeds due to deceleration and acceleration, by incorporating rounded corners, mitigates the problem of overheating of melt pool at corners. This in turn prevents formation of increased depression depths at the corners and thereby formation of pores, as verified through the microscopic observations in Figure 18.

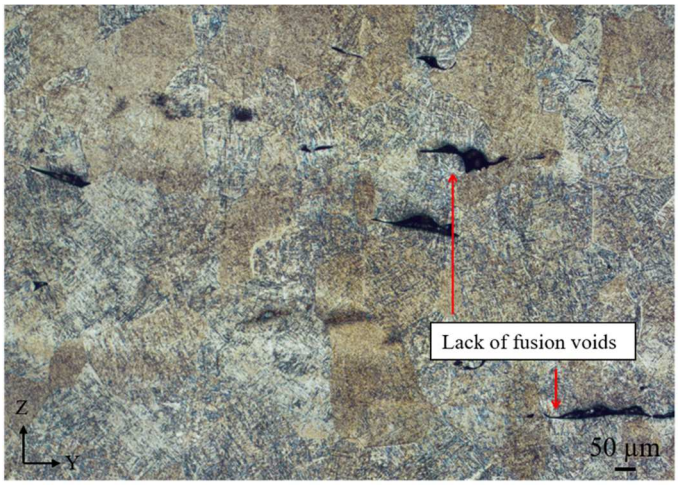

Figure 18: Porosity and lack of fusion defects in 'ZX-Near Corner' zone on cubical shell of 0.5 inches side with rounded corner of fillet 0.5 mm (05-R1) wall section.

Figure 18 shows that lack of fusion voids and porosity on wall section extracted from cubical shell of 0.5 inches side with rounded corner of fillet 0.5 mm (05-R1) have reduced

considerably compared to defects seen in Figure 17. This is consistent with defect density measurement data reported in Figure 12 (b). It is important to note that both images have been captured on 'ZX-Near Corner' zones. Steady state transition of vapor depression at rounded corners decreases instability in the melt pool.

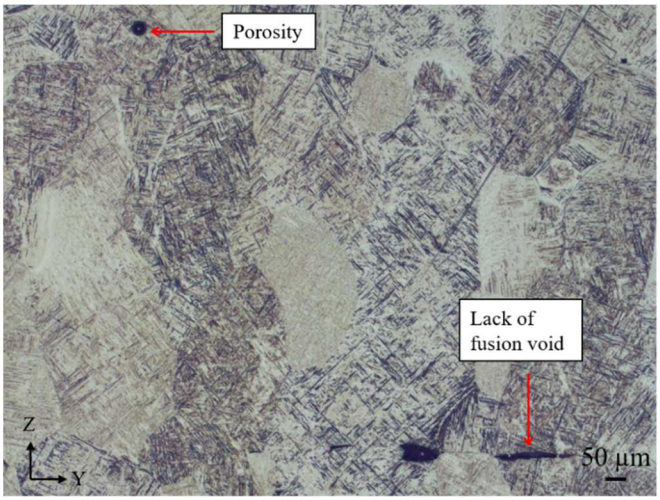

Figure 19: Porosity and lack of fusion defects in 'ZX-Near Corner' zone on cubical shell of 0.5 inches side with rounded corner of fillet 1.0 mm (05-R2) wall section.

Figure 19 shows defects seen in 'ZX-Near Corner' zone on wall section extracted from cubical shell of 0.5 inches side with rounded corner of fillet 1.0 mm (05-R2). Decrease in defect on this section further supports the theory that by giving enough time for layers to fuse, formation of lack of fusion voids is mitigated. Possibility for crack formation is also decreased due to decreased thermal stress at rounded corners.

Incorporation of rounded corners, by facilitating uniform energy input per unit time, leads to reduced defect density as evident from Figures 17-19 and from data plotted in Figure 12(b) and 13(b). Rounding sharp corners improved the homogeneity of microstructure across the deposited layer, as evident from Figure 8.

Chapter 4: Conclusions

Single wall specimens with sharp and rounded corners were manufactured successfully using laser-DED type of additive manufacturing with high disposition rates. Current work demonstrated that by incorporating rounded corners, a consistency in deposition speed is achieved. This consistency in deposition speed improves homogeneity of resulting microstructure and helps to reduce defects in vicinity of turn points.

Samples fabricated using laser-DED show an epitaxial growth of columnar prior β grains in the direction opposite to thermal gradient. Presence of layer bands in the bottom area, which do not coincide with deposited layers, indicate that bottom part of the deposit experienced two or more re-melting cycles beyond the transus temperature line. Top part of the deposit has a mix of colonies and basket weave structure indicating comparatively slow cooling rates. Resulting microstructure is typical as expected for a laser processed Ti6Al4V alloy. Rounding sharp corners led to consistent deposition speeds and hence uniform processing conditions at these turn points. Identical microstructure evolution at turn points as at non-corner positions indicates improved homogeneity in microstructure for shells with rounded corners.

Average hardness of laser-DED deposited shells is comparable throughout indicating that thermal gradients in the deposited part are not large enough to introduce hardness gradient. The representative hardness value on laser deposited sample is 335± 17.5 $HV_{0.1}$. HAZ on laser processed substrate has a finer microstructure which led to 13% increase in hardness.

Macroscopically, shells with and without rounded corners look similar. Slower deposition speeds at corners leads to overheating of melt pool and pore formation as the overheated metal pool entraps surrounding gases. No clear trend in defect density calculations was observed for

measurements in ‘ZX-At Corner’ zone. For ‘ZX-Near Corner’ zone, defect density reduces from 6.8% on cubical shell with sharp corner to nearly full dense areas on shells with rounded corners. Defect density analysis indicate that shells with rounded corner have reduced porosity and lack of fusion voids. Consistent deposition speeds at turn points led to consistent energy input and powder density per unit time. Uniform processing parameters led to reduced defect formation at turn points.

Rounding corners is an effective strategy to improve structural integrity of part. Because the deposition speeds are uniform at turn points, problem of increased powder and power density per unit time is reduced. This is evident from improved homogeneity in resulting microstructure from cubical shells with rounded corners. Rounding corners also reduced defect density, especially in the vicinity of turn points to get near fully dense samples. Incorporating smooth turn points in place of sharp turns in deposition toolpath leads to uniform processing conditions and improved structural integrity.

Chapter 5: Future work

Successfully demonstrated that inclusion of rounded corners improves structural integrity of laser-DED processed parts. Reduced defect density and improved homogeneity in microstructure indicates increased reliability for the part. Future work for further improvement in structural integrity of laser-DED fabricated parts are discussed in the following sections.

5.1 Critical radius for rounded radius

Current study estimated the values for fillet radius for sharp corners by measuring extent of defects across the sample wall from corner edge. It is suggested that further studies be done to investigate minimum critical radius required for rounded corners to achieve consistent deposition speeds by taking into account other factors such as desired deposition speed, motion controller kinematics, etc. A minimum critical radius ensures that changes to initial desired design are minimal.

5.2 Process parameter optimization

It is not possible to minimize defects by geometry optimization alone. While pores are formed due to increased input energy, lack of fusion voids are reduced with increased laser power. The final part quality also depends on processing parameters used during fabrication. It is suggested that a parameter optimization study coupled with geometry optimization be done to get the best of both approaches. Thermal imaging setup can be used to monitor and control melt-pool area by changing processing parameters in real time. This closed loop control systems can change the processing parameters to have uniform processing conditions at turn points.

5.3 Process, structure and property relationship investigation

Samples with rounded corners showed improved homogeneity in resulting microstructure. Consistent disposition speeds, and hence consistent energy inputs, leads to overall consistent microstructure across a layer. Processing parameters have a direct impact on the thermal history of deposited layer and hence control over the resulting microstructure. Microstructure dictates mechanical properties such as hardness, fatigue, tensile strength, etc. It is suggested that further studies be done to explore the coupled relationship among process, structure and mechanical property more thoroughly.

APPENDICES

APPENDIX A: Vickers hardness measurement

Vickers hardness test uses a parallelogram shaped diamond indenter. The included opposite angles are 136° apart. Vickers hardness number (VHN) is defined as ratio of load to the surface area of indentation. It is also referred as Diamond Pyramid Hardness (DPH). The Vickers hardness number can be calculated using the following equation,

$$\text{VHN} = \frac{1.854P}{L^2}$$

where, P and L is the applied load (kg) and average length (mm) of diagonals.

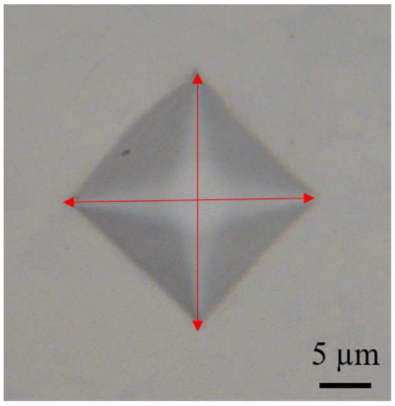

Figure 20: Micro-Vickers hardness indentation on polished Ti6Al4V substrate.

Figure 20 shows an optical image of a typical micro-Vickers hardness indentation for a load of 100 grams. The two diagonal lengths are indicated by red arrows. The test is independent of load values and requires polished surface finishes to avoid errors due to surface roughness. Load values are generally between 1 to 120 kgs and the test is called Vickers microhardness if load value of less than 2 kg is used. The current study uses a constant load of 100 grams with dwell time of 15 sec and follows ASTM E9282 standard test method for hardness measurements.

APPENDIX B: Defect density measurement

Defect density can be defined as the ratio of area of defects in a selected area of interest to the total selected area. Defect density measurements were done on polished wall sections using the area measurement feature available on most optical microscopes.

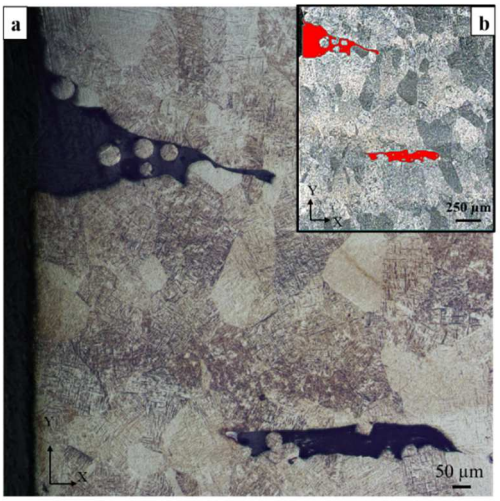

Figure 21: Defect density measurement on wall section using optical microscope (a) defining Area of interest (AOI) and (b) Selecting defects in AOI.

As seen in Figure 21(a), Area Of Interest (AOI) is chosen. In this work, a nominal area of 2 mm × 2 mm was selected on different locations on the wall section of cubical shell to perform defect density analysis. Once area is defined, defects occurring within this area are identified as seen in Figure 21(b). Defects such as pores, lack of fusion voids and cracks that lie within this defined area were selected manually to avoid inclusion of false defects such as scratches. The software then calculates the total area for selected defects and divides it by the area of AOI (4 mm^2 in the current work) to output the defect density number as percentage area of defects. Several such measurements are taken to obtain an average value of defect density.

REFERENCES

REFERENCES

[1] ASTM International. ISO/ASTM52900-15 Standard Terminology for Additive Manufacturing – General Principles – Terminology. West Conshohocken, PA; ASTM International, 2015

[2] Guo, Nannan, and Ming C. Leu. "Additive manufacturing: technology, applications and research needs." Frontiers of Mechanical Engineering 8, no. 3 (2013): 215-243.

[3] Frazier, W.E., 2014. Metal additive manufacturing: a review. Journal of Materials Engineering and Performance, 23(6), pp.1917-1928.

[4] Xue, L. and Islam, M.U., 2006. Laser consolidation-a novel one-step manufacturing process for making net-shape functional components. National research council of Canada Ottawa (Ontario).

[5] Wolfe, D. and Singh, J., 1998. Functionally gradient ceramic/metallic coatings for gas turbine components by high-energy beams for high-temperature applications. Journal of materials science, 33(14), pp.3677-3692.

[6] Balla, V.K., Bose, S. and Bandyopadhyay, A., 2008. Processing of bulk alumina ceramics using laser engineered net shaping. International Journal of Applied Ceramic Technology, 5(3), pp.234-242.

[7] Liu, R., Wang, Z., Sparks, T., Liou, F. and Newkirk, J., 2017. Aerospace applications of laser additive manufacturing. In Laser additive manufacturing (pp. 351-371). Woodhead Publishing.

[8] Optomec.https://www.optomec.com/wp-content/uploads/2016/04/TopTen-Additive-Manufacturing-Apps.pdf

[9] Bandyopadhyay, A. and Heer, B., 2018. Additive manufacturing of multi-material structures. Materials Science and Engineering: R: Reports, 129, pp.1-16.

[10] Wong, K.V. and Hernandez, A., 2012. A review of additive manufacturing. ISRN Mechanical Engineering, 2012.

[11] Sahasrabudhe, H., Harrison, R., Carpenter, C. and Bandyopadhyay, A., 2015. Stainless steel to titanium bimetallic structure using LENS™. Additive Manufacturing, 5, pp.1-8.

[12] Carroll, B.E., Otis, R.A., Borgonia, J.P., Suh, J.O., Dillon, R.P., Shapiro, A.A., Hofmann, D.C., Liu, Z.K. and Beese, A.M., 2016. Functionally graded material of 304L stainless steel and inconel 625 fabricated by directed energy deposition: Characterization and thermodynamic modeling. Acta Materialia, 108, pp.46-54.

[13] Bobbio, L.D., Otis, R.A., Borgonia, J.P., Dillon, R.P., Shapiro, A.A., Liu, Z.K. and Beese, A.M., 2017. Additive manufacturing of a functionally graded material from Ti-6Al-4V to Invar: Experimental characterization and thermodynamic calculations. Acta Materialia, 127, pp.133-142.

[14] Kelbassa, I., Gasser, A. and Wissenbach, K., 2004, April. Laser cladding as a repair technique for blisks out of titanium and nickel base alloys used in aero engines. In Pacific International Conference on Applications of Lasers and Optics (Vol. 2004, No. 1, p. 503). LIA.

[15] Richter, K.H., Orban, S. and Nowotny, S., 2004, October. Laser cladding of the titanium alloy Ti6242 to restore damaged blades. In International Congress on Applications of Lasers & Electro-Optics (Vol. 2004, No. 1, p. 1506). LIA.

[16] Carroll, B.E., Palmer, T.A. and Beese, A.M., 2015. Anisotropic tensile behavior of Ti–6Al–4V components fabricated with directed energy deposition additive manufacturing. Acta Materialia, 87, pp.309-320.

[17] Bian, L., Thompson, S.M. and Shamsaei, N., 2015. Mechanical properties and microstructural features of direct laser-deposited Ti-6Al-4V. JOM 67(3), pp.629-638.

[18] Wang, Z., Palmer, T.A. and Beese, A.M., 2016. Effect of processing parameters on microstructure and tensile properties of austenitic stainless steel 304L made by directed energy deposition additive manufacturing. Acta Materialia, 110, pp.226-235.

[19] Shamsaei, N., Yadollahi, A., Bian, L. and Thompson, S.M., 2015. An overview of Direct Laser Deposition for additive manufacturing; Part II: Mechanical behavior, process parameter optimization and control. Additive Manufacturing, 8, pp.12-35.

[20] Ding, D., Pan, Z., Cuiuri, D. and Li, H., 2015. Wire-feed additive manufacturing of metal components: technologies, developments and future interests. The International Journal of Advanced Manufacturing Technology, 81(1-4), pp.465-481.

[21] Jin, Y.A., He, Y., Fu, J.Z., Gan, W.F. and Lin, Z.W., 2014. Optimization of tool-path generation for material extrusion-based additive manufacturing technology. Additive manufacturing, 1, pp.32-47.

[22] Tang, L., Ruan, J., Landers, R.G. and Liou, F., 2008. Variable powder flow rate control in laser metal deposition processes. Journal of Manufacturing Science and Engineering, 130(4), p.041016.

[23] Goldak, J., Chakravarti, A. and Bibby, M., 1984. A new finite element model for welding heat sources. Metallurgical transactions B, 15(2), pp.299-305.

[24] Wirth, F., Eisenbarth, D. and Wegener, K., 2016. Absorptivity measurements and heat source modeling to simulate laser cladding. Physics Procedia, 83, pp.1424-1434.

[25] Chikarakara, E., Naher, S. and Brabazon, D., 2012. High speed laser surface modification of Ti–6Al–4V. Surface and Coatings Technology, 206(14), pp.3223-3229.

[26] Facchini, L., Magalini, E., Robotti, P., Molinari, A., Höges, S. and Wissenbach, K., 2010. Ductility of a Ti-6Al-4V alloy produced by selective laser melting of prealloyed powders. Rapid Prototyping Journal, 16(6), pp.450-459.

[27] Brandl, E., Schoberth, A. and Leyens, C., 2012. Morphology, microstructure, and hardness of titanium (Ti-6Al-4V) blocks deposited by wire-feed additive layer manufacturing (ALM). Materials Science and Engineering: A, 532, pp.295-307.

[28] Baufeld, B., Brandl, E. and Van der Biest, O., 2011. Wire based additive layer manufacturing: Comparison of microstructure and mechanical properties of Ti–6Al–4V components fabricated by laser-beam deposition and shaped metal deposition. Journal of Materials Processing Technology, 211(6), pp.1146-1158.

[29] Mok, S.H., Bi, G., Folkes, J., Pashby, I. and Segal, J., 2008. Deposition of Ti–6Al–4V using a high power diode laser and wire, Part II: Investigation on the mechanical properties. Surface and Coatings Technology, 202(19), pp.4613-4619.

[30] Murr, L.E., Gaytan, S.M., Medina, F., Martinez, E., Martinez, J.L., Hernandez, D.H., Machado, B.I., Ramirez, D.A. and Wicker, R.B., 2010. Characterization of Ti–6Al–4V open cellular foams fabricated by additive manufacturing using electron beam melting. Materials Science and Engineering: A, 527(7-8), pp.1861-1868.

[31] Brandl, E., Baufeld, B., Leyens, C. and Gault, R., 2010. Additive manufactured Ti-6Al-4V using welding wire: comparison of laser and arc beam deposition and evaluation with respect to aerospace material specifications. Phys. Procedia, 5(Pt 2), pp.595-606.

[32] Baufeld, B., Van der Biest, O. and Gault, R., 2010. Additive manufacturing of Ti–6Al–4V components by shaped metal deposition: microstructure and mechanical properties. Materials & Design, 31, pp.S106-S111.

[33] Javidani, M., Arreguin-Zavala, J., Danovitch, J., Tian, Y. and Brochu, M., 2017. Additive manufacturing of AlSi10Mg alloy using direct energy deposition: Microstructure and hardness characterization. Journal of Thermal Spray Technology, 26(4), pp.587-597.

[34] Kok, Y., Tan, X., Tor, S.B. and Chua, C.K., 2015. Fabrication and microstructural characterisation of additive manufactured Ti-6Al-4V parts by electron beam melting: This paper reports that the microstructure and micro-hardness of an EMB part is thickness dependent. Virtual and Physical Prototyping, 10(1), pp.13-21.

[35] Quintino, L., Costa, A., Miranda, R., Yapp, D., Kumar, V. and Kong, C.J., 2007. Welding with high power fiber lasers–A preliminary study. Materials & Design, 28(4), pp.1231-1237.

[36] Cao, X. and Jahazi, M., 2009. Effect of welding speed on butt joint quality of Ti–6Al–4V alloy welded using a high-power Nd: YAG laser. Optics and Lasers in Engineering, 47(11), pp.1231-1241.

[37] Wang, Q., Li, J., Gouge, M., Nassar, A.R., Michaleris, P.P. and Reutzel, E.W., 2017. Physics-based multivariable modeling and feedback linearization control of melt-pool geometry and temperature in directed energy deposition. Journal of Manufacturing Science and Engineering, 139(2), p.021013.

[38] Benyounis, K.Y., Olabi, A.G. and Hashmi, M.S.J., 2005. Effect of laser welding parameters on the heat input and weld-bead profile. Journal of materials processing technology, 164, pp.978-985.

[39] Martin, A.A., Calta, N.P., Khairallah, S.A., Wang, J., Depond, P.J., Fong, A.Y., Thampy, V., Guss, G.M., Kiss, A.M., Stone, K.H. and Tassone, C.J., 2019. Dynamics of pore formation during laser powder bed fusion additive manufacturing. Nature communications, 10(1), p.1987.

[40] Mukherjee, T. and DebRoy, T., 2018. Mitigation of lack of fusion defects in powder bed fusion additive manufacturing. Journal of Manufacturing Processes, 36, pp.442-449.

[41] Chen, Y., Zhang, K., Huang, J., Hosseini, S.R.E. and Li, Z., 2016. Characterization of heat affected zone liquation cracking in laser additive manufacturing of Inconel 718. Materials & Design, 90, pp.586-594.

[42] Cain, V., Thijs, L., Van Humbeeck, J., Van Hooreweder, B. and Knutsen, R., 2015. Crack propagation and fracture toughness of Ti6Al4V alloy produced by selective laser melting. Additive Manufacturing, 5, pp.68-76.